

RESEARCH ARTICLE | MARCH 05 2024

Carbon-related donor–acceptor pair transition in the infrared in h-BN

M. Almohammad ; Z. Alemoush ; J. Li ; J. Y. Lin  ; H. X. Jiang  

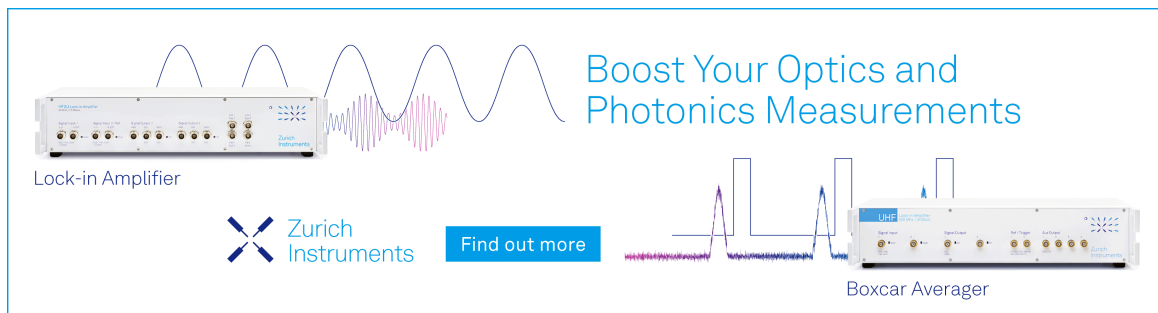


Appl. Phys. Lett. 124, 102106 (2024)

<https://doi.org/10.1063/5.0196810>



CrossMark



Boost Your Optics and Photonics Measurements

Lock-in Amplifier

Zurich Instruments

Find out more

Boxcar Averager

Carbon-related donor-acceptor pair transition in the infrared in h-BN

Cite as: Appl. Phys. Lett. **124**, 102106 (2024); doi: [10.1063/5.0196810](https://doi.org/10.1063/5.0196810)

Submitted: 9 January 2024 · Accepted: 23 February 2024 ·

Published Online: 5 March 2024



View Online



Export Citation



CrossMark

M. Almomhammad, Z. Alemoush, J. Li, J. Y. Lin, ^{a)} and H. X. Jiang ^{a)}

AFFILIATIONS

Department of Electrical and Computer Engineering, Texas Tech University, Lubbock, Texas 79409, USA

^{a)} Authors to whom correspondence should be addressed: hx.jiang@ttu.edu and jingyu.lin@ttu.edu

ABSTRACT

Experimental studies of intentionally doped impurities for the understanding of conductivity control in hexagonal boron nitride (h-BN) ultrawide bandgap (UWBG) semiconductor are limited but are highly desired for emerging applications of h-BN. We report synthesis by hydride vapor phase epitaxy and comparison photoluminescence (PL) emission spectroscopy studies of intentionally carbon (C)-doped and undoped h-BN semi-bulk crystals. In addition to the well-known C-related emission lines observed previously, a C-impurity-related transition near 1.31 eV consisting of multiple phonon replicas has been observed in C-doped h-BN at room temperature. Phonon replicas involved in the 1.31 eV emission have been identified using polarization resolve PL spectroscopy as the transverse acoustic (TA)/longitudinal acoustic (LA) and out-of-plane optical phonon (ZO) modes at the middle point, T, between the Γ - and K-points in the first Brillouin zone. Based on the agreement between the spectral peak position of the observed dominant emission line at 1.31 eV and the calculated energy-level separation between C_B donor (carbon replacing boron) and C_i acceptor (carbon interstitial), the observed IR emission line can be decisively assigned to the donor-acceptor pair (DAP) transition involving the C_B donor and C_i acceptor assisted by the intervalley ($K \rightarrow M$) scattering processes. The results reinforce the perception that C impurities form deep-level centers and provided an improved understanding of C impurities in h-BN.

Published under an exclusive license by AIP Publishing. <https://doi.org/10.1063/5.0196810>

Hexagonal boron nitride (h-BN) is the least studied among III-nitride semiconductors. However, it possesses some exceptional properties including an ultrawide energy bandgap (UWBG, $E_g \sim 6$ eV),^{1–5} high breakdown field,⁶ and excellent thermal properties.⁷ Due to its close lattice match to graphite and chemical inertness, single or a few layers of h-BN have been widely employed as an ideal template, insulating layer, and barrier material for the construction of novel structures such as graphene-based two-dimensional (2D) heterostructures and twisted h-BN with rich physics.^{8–11} Many of the prior experimental studies pertaining to the fundamental properties of h-BN were carried out from millimeter-sized h-BN bulk crystals synthesized by high pressure/high temperature (HPHT) or metal flux method or from single (or a few layers of) h-BN exfoliated from these materials.^{4–10} In the thin film form, h-BN epitaxial layers exhibit some interesting 2D optical properties, such as an extraordinarily high above bandgap optical absorption¹² and ability of tuning several fundamental parameters (including the bandgap, binding energy of exciton and impurities and electron-phonon coupling strength) via the layer number variation.^{13,14} It was shown that a thin film with h-BN layer number exceeding 100 (or thickness ≥ 33 nm) can generally be considered as a

bulk semiconductor.¹⁴ However, to utilize h-BN as an UWBG semiconductor for optoelectronic and electronic device applications, the capabilities for synthesizing wafer-scale bulk materials and doping control are highly desired. More recently, progress toward synthesizing h-BN wafers with a size up to 4-in. in diameter and large thicknesses (or semi-bulk wafers) has been made, and thermal neutron detectors fabricated from 100 μm thick B-10 enriched h-BN wafers have demonstrated a record high detection efficiency^{15,16} by exploiting the unique property of high thermal neutron capture cross section of its atomic constituent B-10 elements.^{17,18}

Carbon (C) is a common impurity in group-III nitride semiconductors, which can be introduced unintentionally from reaction precursors during growth for thin film growth techniques such as metal-organic chemical vapor deposition (MOCVD) or bulk growth techniques including HPHT or metal flux method and could significantly impact their electrical and optical properties. In GaN, it has been found that C impurities can occupy Ga sites (C_{Ga}), acting as shallow donors and nitrogen sites (C_N) as well as interstitial sites acting as deep acceptors.^{19,20} Carbon impurities in AlN have also been extensively investigated during the development of deep UV emitters.²¹

For h-BN, theoretical and experimental studies dedicated to the understanding of various impurities and defects for conductivity control have been limited.^{22–26} Si was shown to incorporate substitutionally on boron site (Si_B) with an activation energy of 1.2 eV,^{22,23} while oxygen impurities tend to substitute nitrogen sites (O_N) behaving as donors with an activation energy of about 0.6 eV,^{25,26} both of which appear to be not ideal dopant candidates in terms of conductivity control in h-BN. Photocurrent excitation spectroscopy was conducted on an intentionally C-doped h-BN epitaxial layer of 30 nm in thickness produced by MOCVD,²⁴ from which a band diagram concerning C impurities in h-BN was constructed, inferring that C-doping introduces both substitutional donors consisting of C occupying the boron site (C_B) and deep acceptors consisting of C occupying the nitrogen sites (C_N) via self-compensation, and that the energy level of carbon donors appears to be too deep to enable carbon as a viable candidate as an n-type dopant in h-BN. A recent first-principles calculation predicated that C could incorporate as C_B , C_N , as well as an interstitial acceptor, C_i ,²⁶ with energy levels of 3.71, 3.19, and 2.40 eV measured with respect to the valence band edge, respectively. While sharp emission lines in the UV and visible spectral regions attributing to the atomic-like features of C-related defects (e.g., C and native defect complexes) have been observed in single or a few layers of h-BN and are considered as potential candidates for robust room-temperature single-photon sources and qubits,^{27–38} so far there have not been sufficient experimental studies to reveal the properties of carbon-related impurities/defects and their implications on the conductivity control in h-BN.

To utilize h-BN as an electronic material, based on the development of III-nitride wide bandgap (WBG) semiconductors, gaining a better understanding of the properties of intentionally doped carbon impurities will be useful to provide insights for their utilization or elimination so that the full potential of h-BN as an UWBG semiconductor can be exploited for emerging practical applications. In this work, we report the synthesis by hydride vapor phase epitaxy (HVPE) and photoluminescence (PL) emission spectroscopy studies of intentionally

C-doped h-BN semi-bulk crystals in the band edge and infrared (IR) spectral regions. Together with the calculated energy levels of C-related impurities in h-BN,²⁶ the observed emission line at 1.31 eV can be attributed to a donor-acceptor pair (DAP) transition involving C_B donors and interstitial acceptors (C_i).

HVPE growth is an established technique for producing wafer scale semi-bulk GaN crystals with large thicknesses at a high growth rate. Compared to MOCVD, precursors for HVPE growth are carbon free, making intentional and controlled doping with carbon impurities possible. Recently, the HVPE growth technique has been employed to produce GaN vertical p-n junction devices with a significantly improved p-type conductivity control through the elimination of the residue carbon impurities.^{39,40} To produce h-BN by HVPE, natural boron trichloride (BCl_3) and NH_3 were used as B and N precursors, respectively, and hydrogen was used as a carrier gas.¹⁶ The growth was conducted on c-plane sapphire of 2-in. in diameter. Due to its layered structure, h-BN self-separates from sapphire to form a freestanding wafer after growth during cooling down.^{15,16} These wafers were then diced into various sizes and shapes for characterization and device fabrication. A micrograph of the h-BN sample used in this study is shown in the inset of Fig. 1(a) and has a thickness of $\sim 100 \mu\text{m}$. Figure 1(a) plots the carbon concentration as a function of the sample depth, probed by secondary-ion mass spectrometry (SIMS). Since the growth and doping conditions remained the same during the growth process, the doping concentration of about 4×10^{20} atoms/ cm^3 at $3 \mu\text{m}$ depth should represent closely the doping concentration in the sample's interior, by neglecting the artifacts induced by the surface of the as-grown h-BN:C sample in SIMS results. Figure 1(b) shows an x-ray diffraction (XRD) spectrum in θ - 2θ scan, revealing a single (002) peak at 26.6° , corresponding to a nearly pure hexagonal phase of BN. The observed h-BN (002) peak position here is slightly lower than that seen in undoped h-BN at 26.7° ,¹⁶ which is most likely related to a high C doping level that impacted the overall crystalline quality of the h-BN:C sample used here. Figure 1(c) shows the room temperature Raman

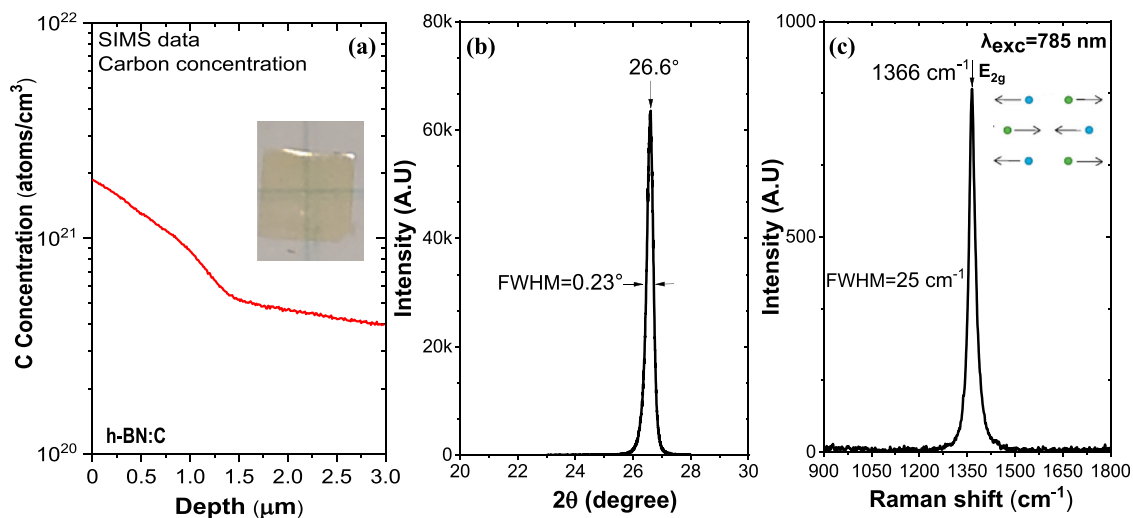


FIG. 1. (a) Carbon concentration profile in a carbon-doped h-BN freestanding sample (h-BN:C) probed by SIMS. The inset shows a micrograph of a freestanding h-BN:C sample of $100 \mu\text{m}$ in thickness used in this study. (b) X-ray diffraction (XRD) spectrum in θ - 2θ scan and (c) room temperature Raman spectrum under 785 nm excitation of the sample used in this study.

spectrum of this freestanding semi-bulk sample. It is interesting to note that the observed Raman peak in this sample is at a lower phonon frequency compared to those observed in the monolayer, few-layer, and thin epitaxial layer on substrates, which are generally under strain.⁴¹ The observed mode at $\Delta\sigma = 1366 \text{ cm}^{-1}$ corresponds well with the Raman peak of bulk h-BN,⁴¹ which is related to the E_{2g} vibration mode (in-plane stretch of B and N atoms) as illustrated in the inset of Fig. 1(c). However, the observed spectral linewidth of 25 cm^{-1} is broad than a typical value of $< 10 \text{ cm}^{-1}$ observed in the monolayer and few-layer BN exfoliated from small bulk crystals. Since the linewidth of a Raman spectrum is directly correlated with the crystalline quality, the result also infers to the fact that there is still a lot of room for improvement in crystalline quality of the h-BN semi-bulk crystals.

To probe carbon impurity-related photoluminescence (PL) emission lines, a frequency quadrupled Ti:sapphire laser with the fourth harmonic photon energy set at 195 nm was used as an excitation source to provide an above bandgap excitation, and a micro-channel plate photomultiplier tube (MCP-PMT) was used to detect PL in the UV spectral region. Figure 2(a) shows the PL emission spectrum measured for a C-doped h-BN sample, revealing two emission lines near 4.1 and 3.9 eV, and another much weaker emission line near 5.5 eV. The 4.1 eV line has been identified to be associated with the presence of C_N .^{24,42,43} However, recent theoretical studies suggested that C_N may not be the origin of the 4.1 eV line, and that its origin is more likely related to the carbon dimer defect C_2 .^{37,44} A hall mark of optical emissions in h-BN is the involvement of a very strong carrier-phonon interaction to conserve the momentum and to enhance the transition probabilities, because of its indirect energy bandgap nature.^{3,45,46} A lower energy peak appearing around 3.9 eV is most likely the phonon replica of the zero-phonon line (ZPL) at 4.1 eV. The phonon involved is close to the known value of the 200 meV longitudinal optical (LO) phonon mode in h-BN.^{45,46} The weak and broad emission line near 5.5 eV seen in the C-doped sample has been attributed previously to the combination of quasi donor-acceptor pair (q-DAP) and impurity-bound exciton transitions in h-BN.⁴⁷ For comparison, PL emission spectrum of an undoped h-BN wafer produced by HVPE is presented in Fig. 2(b), which exhibits a dominant emission line near 3.6 eV

related to the presence of B-vacancy defects⁴⁸ and a weak emission peak near 5.9 eV due to the excitonic transition in h-BN.^{1,3} It is worth noting that the emission lines near 4.1 and 5.5 eV, often observed in MOCVD-grown h-BN epitaxial films and in millimeter-sized h-BN bulk crystals, are hardly visible in undoped h-BN wafers grown by HVPE.

While PL emission properties of h-BN in the UV region have been extensively investigated, emission characteristics in the infrared (IR) spectral region need to be measured to probe possible transitions between defect levels. Room temperature PL emission spectra of a h-BN:C sample measured in the IR spectral region using above ($\lambda_{\text{exc}} = 195 \text{ nm}$) and below ($\lambda_{\text{exc}} = 405 \text{ nm}$) bandgap excitation are shown in Fig. 3(a) using the measurement configuration shown in Fig. 2(c). We noted that the spectrum contains no visible features in the IR region between 0.9 and 1.4 eV under an above bandgap excitation ($\lambda_{\text{exc}} = 195 \text{ nm}$) for both C-doped and undoped h-BN samples. In contrast, the emission spectrum shown in Fig. 3(a) for C-doped sample exhibits a broad emission band with the main peak appearing at 1.31 eV under a below bandgap excitation ($\lambda_{\text{exc}} = 405 \text{ nm}$), while no emission lines were evident in undoped h-BN in the same IR region under the same experimental measurement conditions. More careful inspection of the IR spectrum shown in Fig. 3(a) reveals that the observed emission band comprises multiple emission lines with an equal energy separation of $\sim 80 \text{ meV}$ between two adjacent peaks, while a multiple Gaussian peak fitting provides a separation energy of $\sim 78 \text{ meV}$. It was also shown that deep-level impurity emission lines in h-BN are strongly assisted by the intervalley phonon scattering processes.⁴⁹ We thus attribute this series of emission lines to the same C-impurity-related emission, which has its primary peak at 1.31 eV along with its higher-order phonon replicas, displaying a successive reduction in the emission intensity with increasing the numbers of phonon involved.

The detailed phonon dispersions for the longitudinal acoustic (LA), transverse acoustic (TA), and out-of-plane optical (ZO) phonon branches in h-BN are plotted in Fig. 3(b), revealing a substantial overlap among LA, TA, and ZO phonon modes at the middle of the Brillouin zone (BZ), near the T-point.^{45,46} By examining Fig. 3(b), the

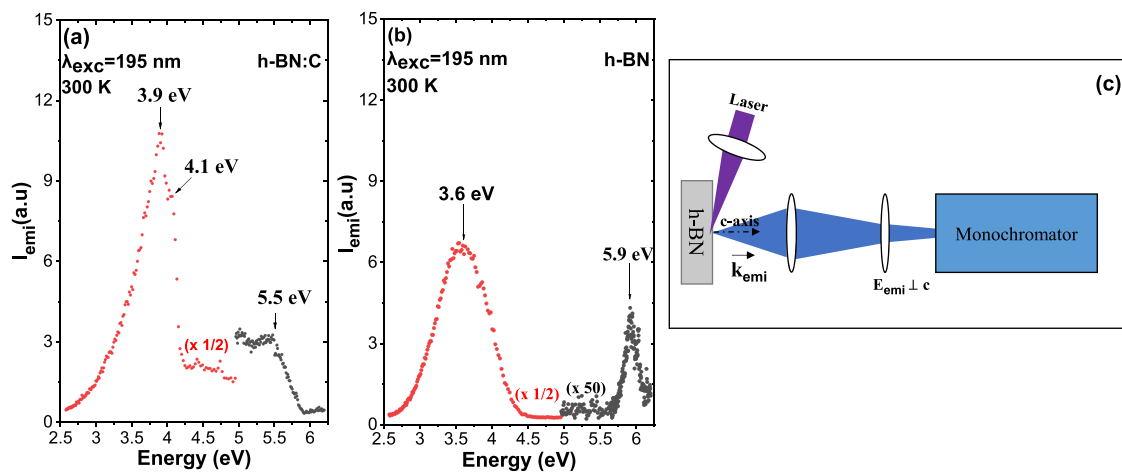


FIG. 2. Room temperature PL emission spectra obtained under an above bandgap excitation ($\lambda_{\text{exc}} = 195 \text{ nm}$) for (a) carbon-doped h-BN (h-BN:C) and (b) undoped h-BN samples. A micro-channel plate photomultiplier tube (MCP-PMT) was used to detect PL in the UV spectral region. (c) Schematic of PL emission spectroscopy measurement setup.

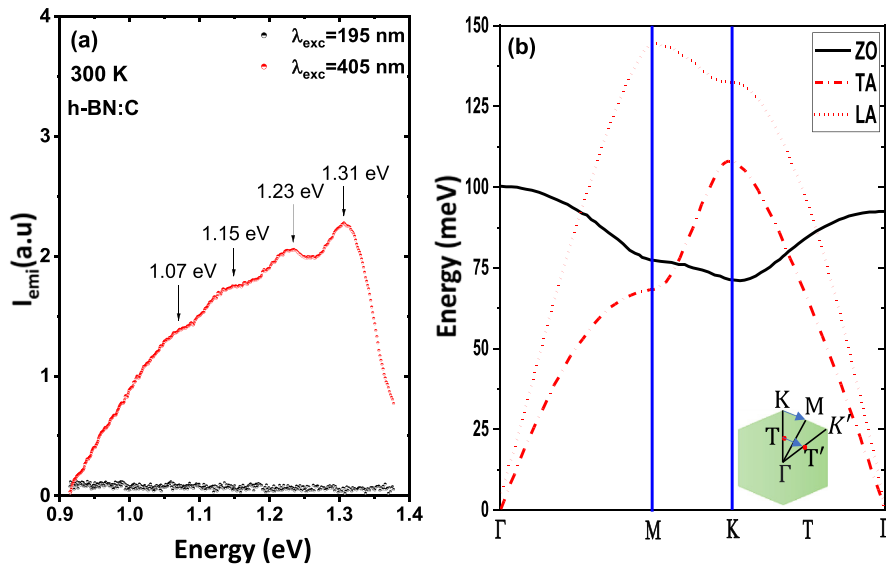


FIG. 3. (a) Room temperature PL emission spectra of a carbon-doped h-BN (h-BN:C) measured in the IR spectral region using above ($\lambda_{\text{exc}} = 195$ nm) and below ($\lambda_{\text{exc}} = 405$ nm) bandgap excitation with the measurement configuration shown in Fig. 2(c). An InGaAs detector was used to collect the PL spectra in the IR spectral region. (b) LA, TA, and ZO phonon dispersion relations of h-BN along the main symmetry directions [Reproduced from Fig. 2(a) of Ref. 45 with permission from Serrano *et al.*, Phys. Rev. Lett. **98**, 095503 (2007)]. The red curves display LA and TA modes polarized in the hexagonal plane, whereas the black curve corresponds to ZO mode polarized along the c-axis. The inset is an illustration of the first Brillouin zone (BZ) of h-BN and high symmetric points of Γ , M, T, and K.

observed phonon energy of ~ 80 meV in Fig. 3(a) is very close to the phonon energies of the LA, TA, and ZO modes near the T-point.^{45,46} However, the ZO phonon replicas are forbidden by symmetry for the experimental configuration shown in Fig. 2(c), in which the wavevector of PL emission is parallel to the c-axis, only allowing the collection of PL emission polarized in the hexagonal plane, $E_{\text{emi}} \perp c$.⁴⁵ Therefore, the phonon replicas of 80 meV observed in the PL emission spectrum shown in Fig. 3(a) can only be attributed to the participation of the LA and TA modes at the T-point. The broad feature of the spectrum and a high background signal appearing in the low energy side of the main peak also suggest possible involvement of more than one phonon branch in the PL emission.

Next, we also checked the possibility for the involvement of out-of-plane phonons in this emission band by performing a polarization resolved PL measurement using an experimental configuration shown schematically in Fig. 4(a), which was made possible by the fact that our

h-BN:C sample is $100 \mu\text{m}$ thick. In the experimental configuration shown in Fig. 4(a), the k-vector of PL emission is perpendicular to the c-axis, but the emitted PL contains both $E_{\text{emi}} // c$ and $E_{\text{emi}} \perp c$ polarization components. A polarizer with E//c orientation was placed in front of the monochromator, allowing the collection of only the PL emission having an $E_{\text{emi}} // c$ polarization orientation. In the configuration of $E_{\text{emi}} // c$, only out-of-plane optical phonon (ZO) and transverse acoustic (ZA) phonon replicas are allowed by symmetry.⁴⁵ The room temperature and 10 K PL spectra measured in the $E_{\text{emi}} // c$ configuration are shown in Figs. 4(b) and 4(c), respectively, which clearly exhibit a shoulder separated by 80–90 meV from the main peak at ~ 1.31 eV, which closely matches the energy of the ZO phonon mode near the T-point, as shown in Fig. 3(b), whereas the energy of ZA phonon mode near the T-point is only around 25 meV.⁴⁵ The long tail in the low energy side implies possible involvement of higher-order ZO phonon replicas, although their spectral peaks are not well resolved.

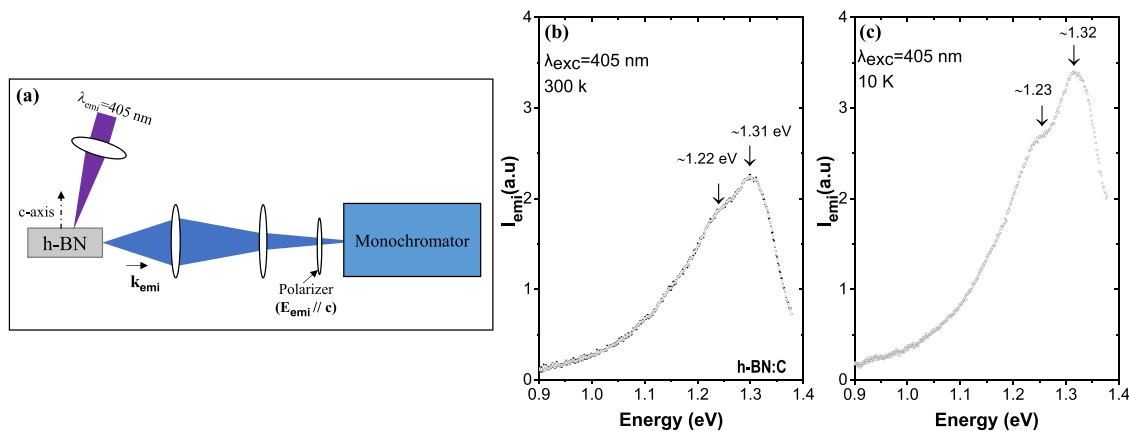


FIG. 4. (a) Schematic of the experimental setup allowing the PL emission to be polarized along the c-axis ($E_{\text{emi}} // c$) by collecting light emission from the sample edge and utilizing a polarizer. (b) Room temperature and (c) 10 K PL spectra of a freestanding h-BN:C sample obtained in the $E_{\text{emi}} // c$ configuration.

It is worth pointing out that the spectral line shape of C-related PL peak near 1.31 eV is not sensitive to temperature due to the deep-level nature of C impurity and broadness of its related emission line, as expected.

The broad spectral line shape of the observed 1.31 eV emission line suggests that its origin is most likely related to a donor–acceptor pair (DAP) recombination. Based on a first-principles calculation of impurities and native defects in h-BN,²⁶ we have constructed in Fig. 5 an energy diagram by including the carbon impurity energy levels for C_B (carbon occupying the boron site) and C_i (carbon interstitial), showing that C_B is located at 3.71 eV above the valence band maximum (VBM), whereas C_i is located at 2.40 eV above VBM. The emission line observed near 1.31 eV in Figs. 3 and 4 corresponds well with the calculated energy-level separation between C_B and C_i of 1.31 eV in h-BN; hence, it can be conclusively assigned to a DAP transition between C_B donors and C_i acceptors, as indicated by the arrow in Fig. 5. The results thus verify the calculated energy levels of C_B and C_i and that carbon impurities form C_B and C_i , which are deep-level impurities in h-BN.²⁶ The absence of the 1.3 eV emission line under the above bandgap excitation can be accounted for by the possibility that other optical recombination channels are more efficient and dominant than this DAP transition.

In h-BN, the conduction band minimum (CBM) and valence band maximum (VBM) are located at M- and K-points in the BZ, respectively.^{1,3,50} It is important to note that both the M- and K-points are located at the edge of the BZ, whereas the T-point is located at the middle point of the Γ -K segment, as illustrated in the inset of Fig. 3.^{1,3,50} The involvement of phonons at the T-point in the 1.31 eV line reveals some interesting insights. Since the CBM of h-BN is located at the M-point and the VBM is at the K-point, an electron (hole) bound to a donor (acceptor) is expected to have a wavefunction maximum near the M- (K-) point. In such a context, it is understandable that a DAP transition involving an electron bounded to the donor associated with the M-point and a hole bounded to the acceptor associated with the K-point is more likely to invoke the participation of phonons with a wave vector pointing from the K-point to M-point, $q = KM$, via intervalley ($K \rightarrow M$) scattering processes.

In summary, intentionally C-doped h-BN semi-bulk crystals have been produced by HVPE. In addition to the well-known

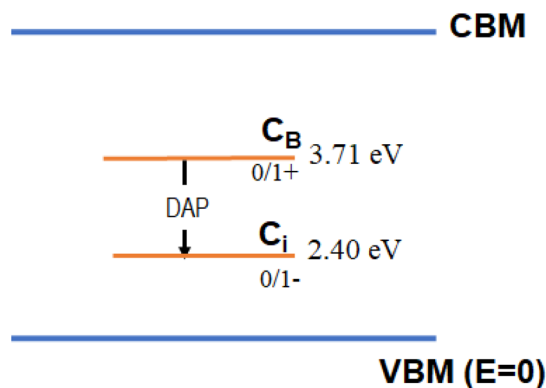


FIG. 5. Energy diagram of carbon impurities relevant to the observed IR emission in h-BN. Energy levels of C_B and C_i with respect the valence band maximum (VBM) are extracted from the results of a first-principles calculation of Ref. 26.

carbon-related emission line near 4.1 eV, a carbon-related transition has been observed in the IR spectral region with the main peak appearing near 1.31 eV. It was further revealed by polarization resolved PL spectroscopy measurements that this transition is assisted by the intervalley ($K \rightarrow M$) scattering processes via phonon modes at the T-point in the first Brillouin zone, including the LA(T)/TA(T) and ZO(T) branches. Based on a previous theoretical study of impurities in h-BN, the IR emission peak at 1.31 eV can be attributed to the donor–acceptor pair recombination with the origin of donors and acceptors being C_B and C_i , respectively. The excellent agreement between the measured and calculated energy separation between C_B and C_i in h-BN reinforces the perception that C-doping tends to introduce deep-level centers, and C is not a viable dopant choice for conductivity control in h-BN.

This research was supported by DOE ARPA-E (DE-AR0001552, monitored by Dr. Olga Spahn and Dr. Eric Carlson). Jiang and Lin are grateful to the AT&T Foundation for the support of Ed Whitacre and Linda Whitacre endowed chairs. The data that support the findings of this study are available within this manuscript.

AUTHOR DECLARATIONS

Conflict of Interest

The authors have no conflicts to disclose.

Author Contributions

Musab Abdallah Almohammad: Data curation (equal); Formal analysis (equal); Investigation (equal); Methodology (equal); Software (equal); Validation (equal); Visualization (equal); Writing – original draft (equal). **Zaid Alemoush:** Data curation (equal); Formal analysis (equal); Investigation (equal); Methodology (equal); Validation (equal). **Jing Li:** Data curation (equal); Formal analysis (equal); Investigation (equal); Methodology (equal); Project administration (equal); Resources (equal); Software (equal); Supervision (equal); Validation (equal); Visualization (equal). **Jingyu Lin:** Conceptualization (equal); Formal analysis (equal); Funding acquisition (equal); Investigation (equal); Methodology (equal); Project administration (equal); Resources (equal); Supervision (equal); Validation (equal); Visualization (equal); Writing – original draft (equal); Writing – review & editing (equal). **Hongxing Jiang:** Conceptualization (equal); Formal analysis (equal); Funding acquisition (equal); Investigation (equal); Methodology (equal); Project administration (equal); Resources (equal); Supervision (equal); Validation (equal); Visualization (equal); Writing – original draft (equal); Writing – review & editing (equal).

DATA AVAILABILITY

The data that support the findings of this study are available within the article.

REFERENCES

1. B. Arnaud, S. Lebègue, P. Rabiller, and M. Alouani, *Phys. Rev. Lett.* **96**, 026402 (2006).
2. T. Sugino, K. Tanioka, S. Kawasaki, and J. Shirafuji, *Jpn. J. Appl. Phys., Part 2* **36**, L463 (1997).
3. G. Cassabois, P. Valvin, and B. Gil, *Nat. Photonics* **10**, 262 (2016).
4. K. Watanabe, T. Taniguchi, and H. Kanda, *Nat. Mater.* **3**, 404 (2004).
5. K. Watanabe, T. Taniguchi, and H. Kanda, *Nat. Photonics* **3**, 591 (2009).

- ⁶A. Ranjan, S. J. O'Shea, A. Padovani *et al.*, *ACS Appl. Electron. Mater.* **3**, 3547 (2021).
- ⁷C. Yuan, J. Li, L. Lindsay, D. Cherns, J. W. Pomeroy, S. Liu, J. H. Edgar, and M. Kuball, *Commun. Phys.* **2**, 43 (2019).
- ⁸C. R. Dean, A. F. Young, I. Meric, C. Lee, L. Wang, S. Sorgenfrei, K. Watanabe, T. Taniguchi, P. Kim, K. L. Shepard, and J. Hone, *Nat. Nanotechnol.* **5**, 722 (2010).
- ⁹C. Dean, A. F. Young, L. Wang, I. Meric, G.-H. Lee, K. Watanabe, T. Taniguchi, K. Shepard, P. Kim, and J. Hone, *Solid State Commun.* **152**, 1275 (2012).
- ¹⁰D. S. Kim, R. C. Dominguez, R. Mayorga-Luna *et al.*, *Nat. Mater.* **23**, 65 (2024).
- ¹¹A. K. Geim and I. V. Grigorieva, *Nature* **499**, 419 (2013).
- ¹²J. Li, S. Majety, R. Dahal, W. P. Zhao, J. Y. Lin, and H. X. Jiang, *Appl. Phys. Lett.* **101**, 171112 (2012).
- ¹³L. Wirtz, A. Marini, M. Gruning, C. Attaccalite, G. Kresse, and A. Rubio, *Phys. Rev. Lett.* **100**, 189701 (2008).
- ¹⁴X. Z. Du, M. R. Uddin, J. Li, J. Y. Lin, and H. X. Jiang, *Appl. Phys. Lett.* **110**, 092102 (2017).
- ¹⁵A. Maity, S. J. Grenadier, J. Li, J. Y. Lin, and H. X. Jiang, *Appl. Phys. Lett.* **116**, 142102 (2020).
- ¹⁶Z. Alemoush, N. K. Hossain, A. Tingsuwatit, M. Almohammad, J. Li, J. Y. Lin, and H. X. Jiang, *Appl. Phys. Lett.* **122**, 012105 (2023).
- ¹⁷O. Osberghaus, *Z. Phys.* **128**, 366 (1950).
- ¹⁸G. F. Knoll, *Radiation Detection and Measurement*, 4th ed. (John Wiley & Sons, 2010).
- ¹⁹A. Armstrong, A. R. Arehart, B. Moran, S. P. DenBaars, U. K. Mishra, J. S. Speck, and S. A. Ringel, *Appl. Phys. Lett.* **84**, 374 (2004).
- ²⁰J. L. Lyons, A. Janotti, and C. G. Van de Walle, *Appl. Phys. Lett.* **97**, 152108 (2010).
- ²¹M. Kneissl, T. Y. Seong, J. Han, and H. Amano, *Nat. Photonics* **13**, 233 (2019).
- ²²F. Oba, A. Togo, I. Tanaka, K. Watanabe, and T. Taniguchi, *Phys. Rev. B* **81**, 075125 (2010).
- ²³S. Majety, T. C. Doan, J. Li, J. Y. Lin, and H. X. Jiang, *AIP Adv.* **3**, 122116 (2013).
- ²⁴M. R. Uddin, J. Li, J. Y. Lin, and H. X. Jiang, *Appl. Phys. Lett.* **110**, 182107 (2017).
- ²⁵S. J. Grenadier, A. Maity, J. Li, J. Y. Lin, and H. X. Jiang, *Appl. Phys. Lett.* **112**, 162103 (2018).
- ²⁶L. Weston, D. Wickramaratne, M. Mackoite, A. Alkauskas, and C. G. Van de Walle, *Phys. Rev. B* **97**, 214104 (2018).
- ²⁷R. Bourrellier, S. Meuret, A. Tararan, O. Stephan, M. Kociak, L. H. G. Tizei, and A. Zobelli, *Nano Lett.* **16**, 4317 (2016).
- ²⁸T. Q. P. Vuong, G. Cassabois, P. Valvin, A. Ouerghi, Y. Chassagneux, C. Voisin, and B. Gil, *Phys. Rev. Lett.* **117**, 097402 (2016).
- ²⁹T. Tran, K. Bray, M. J. Ford, M. Toth, and I. Aharonovich, *Nat. Nanotechnol.* **11**, 37 (2016).
- ³⁰T. T. Tran, C. Elbadawi, D. Totonjian, C. J. Lobo, G. Grosso, H. Moon, D. R. Englund, M. J. Ford, I. Aharonovich, and M. Toth, *ACS Nano* **10**, 7331 (2016).
- ³¹N. Mendelson, D. Chugh, J. R. Reimers, T. S. Cheng, A. Gottscholl, H. Long, C. J. Mellor, A. Zettl, V. Dyakonov, P. H. Beton, S. V. Novikov, C. Jagadish, H. H. Tan, M. J. Ford, M. Toth, C. Bradac, and I. Aharonovich, *Nat. Mater.* **20**, 321 (2021).
- ³²F. Hayee, L. Yu, J. L. Zhang, C. J. Ciccarino, M. Nguyen, A. F. Marshall, I. Aharonovich, J. Vučković, P. Narang, T. F. Heinz, and J. A. Dionne, *Nat. Mater.* **19**, 534 (2020).
- ³³S. N. Grinyaev, F. V. Konusov, and V. V. Lopatin, *Phys. Solid State* **44**, 286 (2002).
- ³⁴A. Sajid and K. S. Thygesen, *2D Mater.* **7**, 031007 (2020).
- ³⁵T. Korona and M. Chojecki, *Int. J. Quantum Chem.* **119**, e25925 (2019).
- ³⁶P. Auburger and A. Gali, *Phys. Rev. B* **104**, 075410 (2021).
- ³⁷M. Maciaszek, L. Razinkovas, and A. Alkauskas, *Phys. Rev. Mater.* **6**, 014005 (2022).
- ³⁸C. Jara, T. Rauch, S. Botti, M. A. L. Marques, A. Norambuena, R. Coto, J. E. Castellanos-Águila, J. R. Maze, and F. Muñoz, *J. Phys. Chem. A* **125**, 1325 (2021).
- ³⁹H. Fujikura, T. Konno, T. Kimura, Y. Narita, and F. Horikir, *Appl. Phys. Lett.* **117**, 012103 (2020).
- ⁴⁰K. Ohnishi, N. Fujimoto, S. Nitta, H. Watanabe, S. Lu, M. Deki, Y. Honda, and H. Amano, *J. Appl. Phys.* **132**, 145703 (2022).
- ⁴¹Q. Cai, D. Scullion, A. Falin, K. Watanabe, T. Taniguchi, Y. Chen, E. J. G. Santos, and L. H. Li, *Nanoscale* **9**, 3059 (2017).
- ⁴²K. Era, F. Minami, and T. Kuzuba, *J. Lumin.* **24–25**, 71 (1981).
- ⁴³T. Pelini, C. Elias, R. Page, L. Xue, S. Liu, J. Li, J. H. Edgar, A. Dréau, V. Jacques, P. Valvin, B. Gil, and G. Cassabois, *Phys. Rev. Mater.* **3**, 094001 (2019).
- ⁴⁴M. Mackoite-Sinkevičienė, M. Maciaszek, C. G. Van de Walle, and A. Alkauskas, *Appl. Phys. Lett.* **115**, 212101 (2019).
- ⁴⁵J. Serrano, A. Bosak, R. Arenal, M. Krisch, K. Watanabe, T. Taniguchi, H. Kanda, A. Rubio, and L. Wirtz, *Phys. Rev. Lett.* **98**, 095503 (2007).
- ⁴⁶T. Q. P. Vuong, G. Cassabois, P. Valvin, V. Jacques, A. Van Der Lee, A. Zobelli, K. Watanabe, T. Taniguchi, and B. Gil, *2D Mater.* **4**, 011004 (2016).
- ⁴⁷L. Mueur and A. Kanaev, *J. Appl. Phys.* **103**, 103520 (2008).
- ⁴⁸Z. Alemoush, A. Tingsuwatit, J. Li, J. Y. Lin, and H. X. Jiang, *Crystals* **13**, 1319 (2023).
- ⁴⁹V. Alexander, I. Weinstein, and D. Zamyatin, *J. Lumin.* **208**, 363 (2019).
- ⁵⁰L. Artús, M. Feneberg, C. Attaccalite, J. H. Edgar, J. Li, R. Goldhahn, and R. Cuscó, *Adv. Photonics Res.* **2**, 2000101 (2021).